J. metamorphic Geol., 2002, **20,** 203–213

Growth of myrmekite coronas by contact metamorphism of granitic mylonites in the aureole of Cima di Vila, Eastern Alps, Italy

B. CESARE,[1,2] C. MARCHESI[1] AND J. A. D. CONNOLLY[3]
[1]*Dipartimento di Mineralogia e Petrologia, Università di Padova. Corso Garibaldi, 37, 35137 Padova, Italy (bernardo@dmp.unipd.it)*
[2]*C.N.R. Centro di Studio per la Geodinamica Alpina, Padova, Italy*
[3]*Department of Earth Sciences, Swiss Federal Institute of Technology, CH-8092 Zurich, Switzerland*

ABSTRACT In the contact aureole of the Oligocene granodiorite of Cima di Vila, granitic pegmatites of Variscan age were strongly deformed during eo-Alpine regional metamorphism, with local development of ultramylonites. In the ultramylonite matrix, consisting of quartz, plagioclase, muscovite and biotite, microstructures show grain growth of quartz within quartz ribbons, and development of decussate arrangements of mica. These features indicate that dynamic recrystallization related to mylonite development was followed by extensive static growth during contact metamorphism. K-feldspar porphyroclasts up to 1.5 cm are mantled by myrmekite that forms a continuous corona with thickness of about 1 mm. In both XZ and YZ sections, myrmekite tubules are undeformed, and symmetrically distributed in the corona, and oligoclase-andesine hosts have random crystallographic orientation. Myrmekite development has been modelled from the *P–T–t* evolution of the ultramylonites, assuming that the development of the ultramylonites occurred during eo-Alpine metamorphism at *c.* 450 °C, 7.5 kbar, followed by contact metamorphism at *c.* 530 °C, 2.75 kbar. Phase diagram pseudosections calculated from the measured bulk composition of granitic pegmatite protolith indicate that the equilibrium assemblage changes from Qtz–Phe–Ab ± Zo ± Cpx ± Kfs during the ultramylonite stage to Qtz–Pl($An_{30–40}$)–Ms–Kfs–Bt(Ann_{55}) during the contact metamorphic stage. The thermodynamic prediction of increasing plagioclase mode and anorthite content, change of white mica composition and growth of biotite, occurring during the end of the heating path, are in agreement with the observed microstructures and analysed phase compositions of ultramylonites. Along with microstructural evidence, this supports the model that K-feldspar replacement by myrmekite took place under static conditions, and was coeval with the static growth accompanying contact metamorphism. Myrmekite associated with muscovite can develop under prograde (up-temperature) conditions in granites involved in polymetamorphism.

Key words: contact metamorphism; Eastern Alps; mylonite; myrmekite.

INTRODUCTION

Myrmekite, the symplectic intergrowth of quartz and plagioclase, is a common constituent of magmatic and metamorphic rocks of granitoid composition (e.g. Phillips, 1974), and is also observed in other rock types, including metapelites (e.g. Vernon, 1978) and metabasites. In most cases, myrmekite is associated with K-feldspar, but in places it is observed to replace albitic plagioclase (Ashworth, 1986). Several genetic processes have been hypothesised as models for myrmekite development, the most popular are that myrmekite forms by replacement of, and exsolution from primary K-feldspar (Becke, 1908, and Schwantke, 1909, respectively). Occasionally the reverse mechanism, myrmekite substitution by K-feldspar, is also observed (Hippert & Valarelli, 1998). A detailed discussion of the different genetic models can be found, for example, in Ashworth (1972) and Phillips (1974, 1980); in this study we are particularly interested in the genetic interpretation of myrmekite in deformed rocks.

Owing to its common occurrence in deformed granitoids (e.g. Vernon, 2000), augengneisses and granitic mylonites (e.g. Simpson, 1985), myrmekite is often considered to be genetically related to strain. Some myrmekite occurrences can confidently be interpreted as deformation-induced, as in the example described by Simpson & Wintsch (1989), where textural evidence indicates syndeformational myrmekite growth. In other instances, myrmekite origins are more equivocal. As discussed by Vernon (1991), strain energy does not seem to be necessary for myrmekite growth,

nor for its nucleation, even if it does catalyze growth kinetics by promoting the access of the intergranular fluid phase to reaction sites.

In this contribution we report on unusual myrmekite coronas around K-feldspar porphyroclasts in some granitic ultramylonites from a contact aureole in the eastern Italian Alps. We show that in this case myrmekite growth is not induced by deformation, but by heating in a static environment during contact metamorphism. Our study takes advantage of the work of Stöckhert (1984, 1987), who studied and dated similar myrmekite-free granitic gneisses outcropping a few kilometres to the west, outside the contact aureole. We utilise Stöckhert's results as a geological scenario to which our data add information about the latest, contact metamorphic event, and from which we can find constraints on the genetic interpretation of myrmekites.

GEOLOGICAL SETTING

The myrmekites occur in mylonitic rocks from the Austroalpine basement of the Eastern Alps (Fig. 1). In the region located between the Tauern Window and the Deferegger–Anterselva–Valles (DAV) line, the Austroalpine basement is polymetamorphic and consists of a pre–Alpine association of high-grade paragneisses, granitic pegmatites, amphibolites, quartzites and marbles (Cesare, 1999 and references therein). These rocks were involved in the polyphase regional Alpine metamorphism, and finally intruded during the Oligocene (Borsi *et al*., 1979) by the granodioritic to tonalitic plutons of Vedrette di Ries (Rieserferner, Bellieni *et al.*, 1981) and Cima di Vila (Zinsnock, Bellieni, 1980). Data (Sassi *et al*., 1980; Prochaska, 1981; Stöckhert, 1984, 1987; Cesare, 1992) indicate a two-stage Alpine cycle, with eo-Alpine metamorphism at *c*. 100 Ma, $P = 7.5 \pm 1.5$ kbar and $T = 450 \pm 50$ °C followed by decompression and late-Alpine metamorphism ('Tauern crystallization') under low-T greenschist facies conditions (350 ± 50 °C). Oligocene contact metamorphism was the last metamorphic event recorded in the area; in the aureole of Vedrette di Ries it occurred at pressures in the range 2.5–3.5 kbar and maximum temperatures of *c.* 620 °C (Cesare, 1994).

Owing to the proximity to the main Alpine suture, metamorphism was accompanied by intense deformation during both the eo-Alpine (Stöckhert, 1987) and the late-Alpine events (Kleinschrodt, 1987). As a result, mylonites are widespread throughout the area, and discrete mylonite zones of considerable thickness and lateral continuity occur far from (and north of) the DAV line. This observation is of primary importance for the kinematic interpretation of the relationships between pluton emplacement and activity of shear zones, as the DAV line is attributed a major role in the emplacement of the Vedrette di Ries and Cima di Vila plutons (e.g. Schmid *et al*., 1989; Müller *et al*., 2000; Steenken *et al*., 2000).

The mylonites where the samples have been collected are located between the Cima di Vila and Vedrette di Ries plutons, and occur within the contact aureole of Cima di Vila, being approximately 700 m north of its contact; the mylonites are *c.* 50 m thick, and can be traced along strike for a few kilometres. The mylonitic foliation has an average orientation of *c.* 80/170°. Despite the widespread occurrence of planar foliations (Fig. 2), the mylonites locally show crenulations and, more significantly, metric isoclinal folds (Fig. 3).

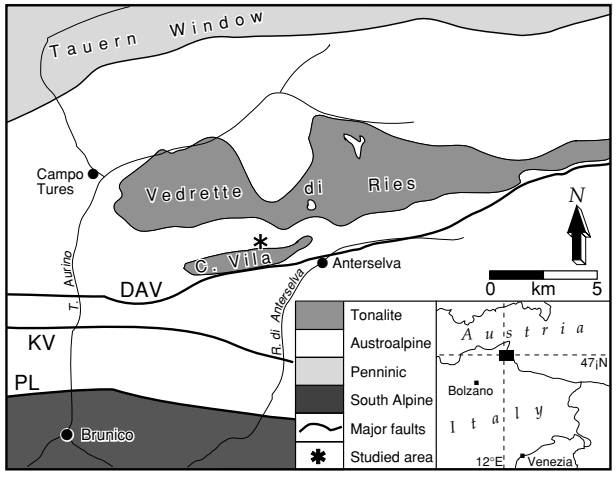

Fig. 1. Geological sketch map of the region of Cima di Vila and Vedrette di Ries plutons, with location of the studied outcrop (after Cesare, 1999). The major tectonic lines are: the Deferegger-Anterselva-Valles (DAV) line, the Kalkstein-Vallarga (KV) line and the Periadriatic Lineament (PL).

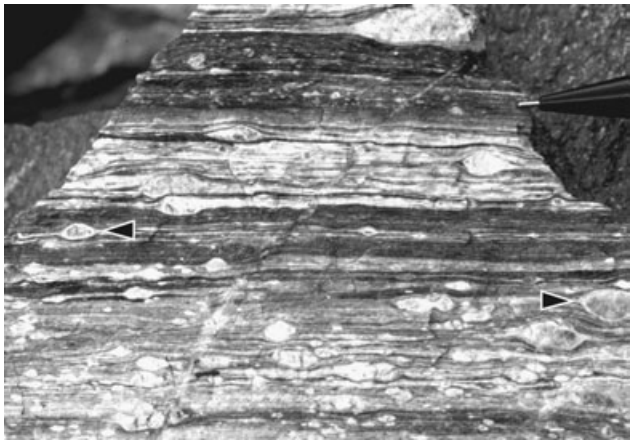

Fig. 2. Hand specimen of a mylonite derived from a pegmatitic orthogneiss, in XZ section. Quartz and feldspar rich layers (white) alternating with mica rich layers (grey) define the mylonitic foliation. Myrmekite coronas (white) occur around some porphyroclasts (arrows).

Fig. 3. Symmetric, M-shaped hinge of a mesoscopic fold involving mylonites derived from pegmatitic orthogneisses and interlayered metapelites.

In agreement with the interpretations of Stöckhert (1984), Mager (1985) and Kleinschrodt (1987), the observations suggest that the mylonitic foliation, of likely eo-Alpine age, was isoclinally folded during the subsequent Alpine evolution.

The mylonite zone primarily involves granitic orthogneisses, derived from a coarse-grained pegmatitic protolith, and minor metapelites; the former have been deformed to mylonites or ultramylonites as classified by K-feldspar porphyroclast abundance. The bulk composition, phase compositions and field relationships of granitic orthogneisses are identical to those of orthogneisses exposed a few kilometres to the west, outside the contact aureoles of Oligocene intrusives; the origin of the pegmatitic protoliths has been dated at *c.* 260 Ma by Borsi *et al.* (1980) by the whole rock Rb–Sr method. Subsequent detailed study and K–Ar dating by Stöckhert (1984, 1987) focused on the microstructural evolution accompanying the Alpine metamorphism of the gneisses, and showed that the eo-Alpine metamorphism occurred at *c.* 100 Ma. If, by analogy, a late-Variscan age can be assumed also for the protolith of the mylonites of the present study, it follows that these have been involved only in the Alpine metamorphic evolution and accompanying deformation events, at the *P–T* conditions reported above. It is noteworthy that the granitic orthogneisses further to the west contain chlorite and epidote, but do not contain myrmekite (Borsi *et al.*, 1980; Stöckhert, 1987).

The pelitic mylonites, which are often interlayered with the granitic mylonites, may contain macroscopic andalusite, up to 4 cm in length, randomly oriented with respect to the main foliation. As andalusite is a typical, and exclusive, contact metamorphic mineral in this region (Cesare, 1992), this suggests that the mylonites formed prior to emplacement of the tonalitic plutons and were subsequently affected by contact metamorphism.

MICROSTRUCTURES

The highly deformed pegmatitic orthogneisses are composed of quartz, plagioclase, muscovite, K-feldspar, biotite and garnet, and have a granitic to 'granodioritic' composition (Table 1), depending on the amount of intermixed pelitic layers.

In hand specimen these rocks show a well-developed mylonitic foliation, defined by alternating quartz ribbons, feldspar-rich and mica-rich layers, which wrap around porphyroclasts up to 1.5 cm in size. The compositional layering is often enhanced by the presence of biotite-rich pelitic beds intercalated with the main layers of granitic composition; in places it is possible to observe a thin white corona around the K-feldspar porphyroclasts, indicating the presence of myrmekite

Table 1. XRF Bulk rock analyses of ultramylonites. All Fe expressed as FeO_{tot}. Samples with $SiO_2 < 70\%$ contain visible intermixed pelitic layers.

Sample	MC2P	MC3	MC9B	MC10P	MC12	VR266
SiO_2	71.37	74.20	73.19	69.04	69.27	68.55
TiO_2	0.37	0.20	0.31	0.59	0.55	0.47
Al_2O_3	13.32	13.19	14.27	13.90	14.57	16.08
FeO_{tot}	3.08	1.12	1.77	4.00	3.47	2.61
MnO	0.10	0.01	0.02	0.06	0.06	0.02
MgO	1.04	0.39	0.62	1.60	1.57	0.96
CaO	2.55	0.59	1.19	1.50	2.07	1.29
Na_2O	1.54	2.02	2.16	1.38	1.92	2.32
K_2O	4.72	6.51	4.04	5.05	4.31	4.71
P_2O_5	0.36	0.09	0.16	0.13	0.15	0.18
L.O.I.	1.06	0.89	1.47	1.90	1.64	2.23
Total	99.50	99.21	99.19	99.16	99.57	99.41

(Fig. 2). The shape of porphyroclasts is flattened and similar in two measured samples, with average X/Y and Y/Z ratios of *c.* 1.55 and *c.* 1.95, respectively. The volume percent of porphyroclasts, estimated in the same samples by image analysis of polished XZ and YZ sections, is between 1.5 and 3.5%, defining the rocks as ultramylonites.

The matrix of the mylonites is formed of quartz, muscovite, plagioclase and biotite in a fine grained ($< 50\ \mu m$) mixture where K-feldspar is absent. In the matrix, quartz microstructures may indicate deformation, dynamic recrystallization and recovery; however, the presence of polygonal granoblastic aggregates, with straight quartz–plagioclase–mica phase boundaries is also observed (Fig. 4a). In the ribbons, quartz displays coarser grain size (300–400 μm), straight grain boundaries and abundant triple junctions, that indicate grain growth processes driven by reduction of interfacial free energy (Fig. 4b). Three generations of both biotite and muscovite are visible: deformed mica-fish (0.5–5 mm), particularly of muscovite, are probably relicts of the protolith; a second generation (50–100 μm) is parallel to the foliation and related to the dynamic recrystallization during mylonitisation; and the youngest generation is represented by fine grained crystals (*c.* 150 μm) that are randomly oriented, cut the earlier generations, and most probably grew during static crystallization. Nodular aggregates of decussate biotite, often preserving garnet relicts, are typical of this static generation (Fig. 4c). Despite wrapping by the mylonitic foliation, the micas are undeformed, suggesting that the growth of decussate biotite as pseudomorphs after garnet post-dates mylonite development. Randomly oriented, subhedral lamellae of fine-grained muscovite are also commonly associated with K-feldspar and myrmekite; we infer that these randomly oriented micas also post-date mylonitisation.

Microperthitic K-feldspar constitutes most of the mylonite porphyroclasts, together with rare mica fish and garnet. K-feldspar has well developed strain shadows and mica-rich strain caps (Fig. 4d), it is sometimes internally deformed and invariably surrounded by myrmekite, even on the terminations that face the supposed incremental stretching direction. YZ (Fig. 4d) and XZ sections show that myrmekite forms a continuous corona of fairly constant thickness of about 1 mm. The corona may be multiple, with two or three concentric shells of myrmekite (Fig. 4e), which sometimes completely replace K-feldspar. Coronas are formed by coalescing, straight, tubular myrmekite (Fig. 4f) oriented normal to the matrix–corona boundary (Fig. 4e). Myrmekite shows neither comma-shaped lobes (e.g. Simpson, 1985) nor internal deformation; the plagioclase host is untwinned, and has maximum length of 1000 μm and aspect ratio of *c.* 5 : 1. The quartz inside myrmekite appears as cylindrical vermicules of constant thickness (*c.* 5–10 μm), with an arborescent pattern radiating from the centre, or parallel to the long side, of the plagioclase host.

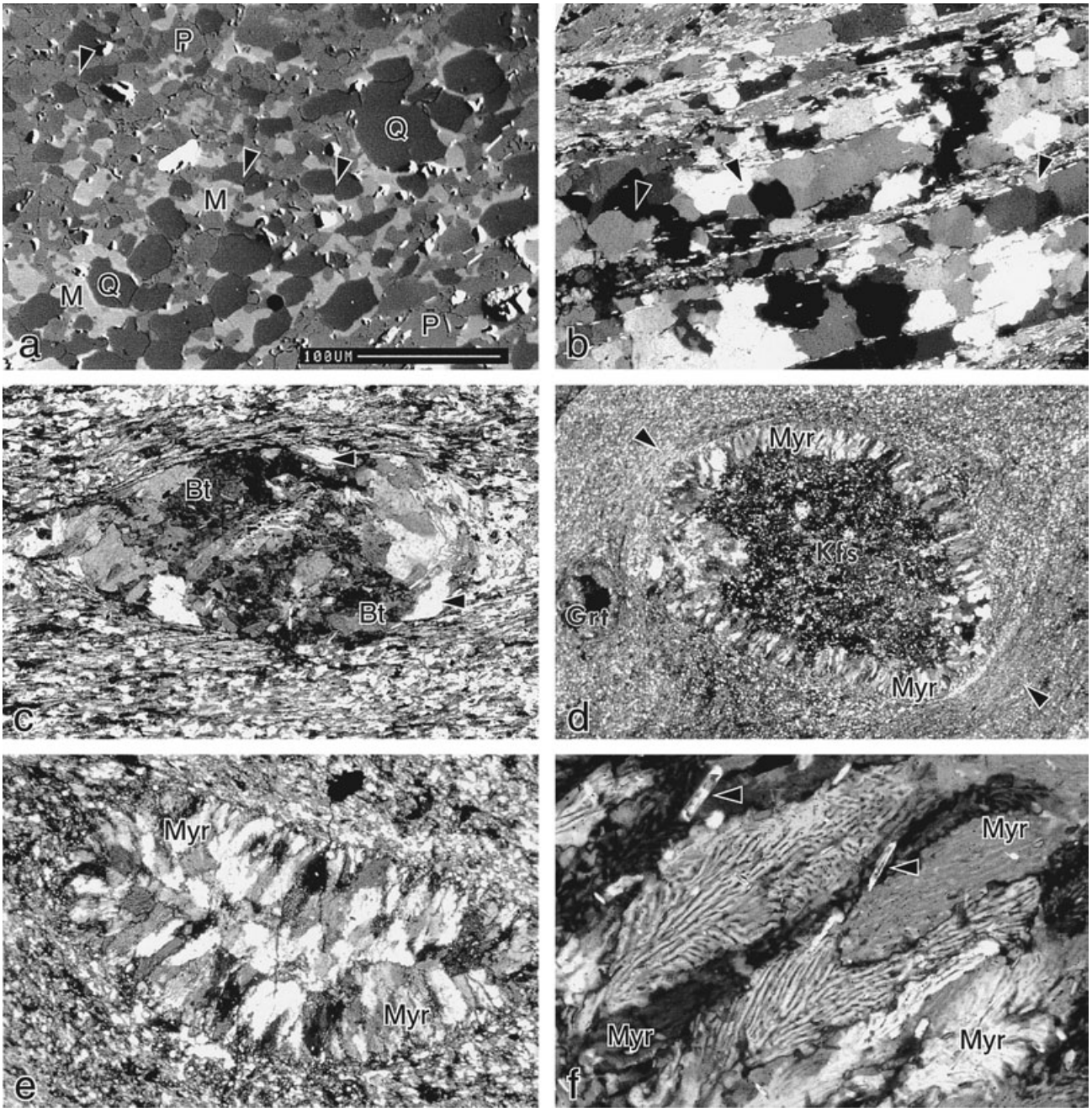

Fig. 4. Microstructures in the pegmatitic ultramylonites. All are optical photomicrographs, except for (a), which is a backscattered electron microscope (BSEM) image. (a) The matrix of this ultramylonites consists of quartz (Q), muscovite (M) and plagioclase (P), and tends to develop an inequigranular polygonal fabric with triple junctions at 120° (arrows). (b) Statically recrystallized quartz ribbons in the mylonite matrix. Inside the ribbons grain boundaries are often straight and the size of quartz is greater than in the matrix due to a process of grain boundary area reduction. Note straight grain boundaries and triple junctions (arrows). Crossed polars (CPL), width of view *c.* 2 mm (c) Decussate aggregate of biotite (Bt), pseudomorph after garnet, wrapped by the subhorizontal mylonitic foliation. Randomly crystallized muscovite also occurs in the decussate aggregate (arrows). Plane-polarised light (PPL).Width of view *c.* 1.5 mm (d) YZ section of a mylonite with an inclusion-rich K-feldspar porphyroclast (Kfs) rimmed by a continuous, about 1 mm thick corona of myrmekite (Myr). Muscovite-rich strain caps are well developed (arrows). A small, resorbed garnet porphyroclast (Grt) is visible on the left. CPL. Width of view 15 mm (e) Myrmekite aggregate forming a composite corona in XZ section. The K-feldspar porphyroclast is not visible because of complete replacement or because the thin section cuts the corona on its edge. Note the disposition of myrmekite: it is essentially normal to the matrix–corona boundary and projects from all sides towards the interior of aggregate. CPL. Width of view 15 mm (f) Detail of the myrmekite corona, showing the straight, elongate shape of plagioclase and the arborescent orientation of quartz vermicules. Small, subhedral, randomly oriented crystals of white mica are also present in the corona (arrows, see also Fig. 5a). CPL. Width of view 0.75 mm.

At the contact with K-feldspar, the myrmekite boundary is irregular and shows no development of crystal faces, suggesting a replacive origin (Phillips, 1980). Towards the matrix, myrmekite is observed in contact with quartz (Fig. 5a) and muscovite, the latter especially along strain caps (Fig. 5b,c). In these microstructures, occurrence of quartz tubules at the immediate contact between myrmekite and any matrix mineral, indicates that preferred nucleation of myrmekite from pre-existing plagioclase, as frequently reported (e.g. Ashworth, 1972; Vernon, 1991), did not occur.

As noted above, fine-grained muscovite occurs also in the myrmekite corona (Figs 4f & 5a), and in the K-feldspar porphyroclast. In places, subhedral, undeformed lamellae of muscovite are located between myrmekite tubules, with (001) planes defining the crystal boundary (Fig. 5d); this intergrowth suggests synchronous crystallization of myrmekite and muscovite.

In the outer part of coronas, myrmekite generally does not show grain-size reduction towards the Qtz–Ms–Pl-bearing mylonitic matrix. Fine-grained aggregates of quartz and plagioclase, possibly representative of myrmekite recrystallization during deformation (Vernon, 1991) are observed only as minor features around porphyroclasts.

The following textural observations indicate that the mylonites underwent post-kinematic metamorphism: granoblastic microstructures of quartz ribbons and quartz-mica matrix, where processes of grain growth are identified; undeformed, subhedral micas at a high angle to the foliation of the matrix; decussate aggregates of biotite undeformed within the

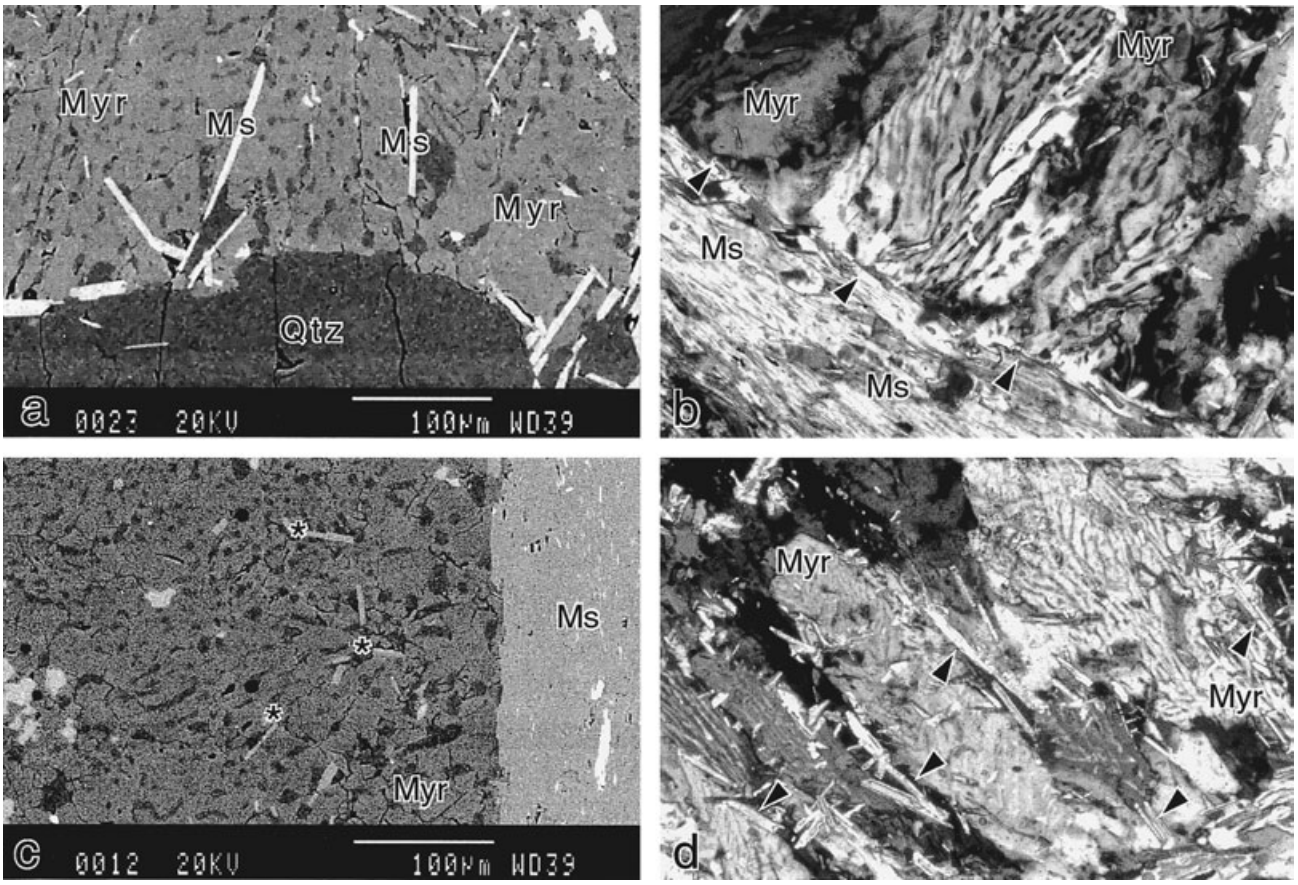

Fig. 5. Details of myrmekite coronas and myrmekite-matrix boundaries. (a) BSEM image showing the contact between myrmekite corona (top half) and quartz (Qtz, bottom). In the myrmekite, quartz blebs are homogeneously distributed up to the boundary towards quartz. The myrmekite contains subhedral lamellae of muscovite (Ms) oriented both parallel and at a high angle to the quartz–myrmekite boundary. (b) Outer limit of a myrmekite corona in contact with a phengite-rich strain cap, where fine-grained mica is aligned along the mylonitic foliation. Numerous muscovite-myrmekite boundaries, with quartz tubules at the immediate contact, can be observed (arrows). CPL. Width of view *c.* 0.5 mm (c) BSEM image showing the outer margin of a myrmekite corona (left side of image) facing a mica-rich strain cap (right) where crystals of phengitic muscovite are strongly aligned. Quartz vermicules appear as dark grey blebs in the myrmekitic plagioclase. Stars indicate subhedral, randomly oriented crystals of muscovite. (d) Subhedral lamellae of muscovite (arrows) in a myrmekite corona. Most muscovite have (001) faces parallel to, or defining, the boundary between myrmekite tubules. CPL. Width of view *c.* 1.2 mm.

mylonitic foliation; continuity and constant thickness of the myrmekite corona; shape, distribution and orientation of myrmekite in the corona. In addition, the limited influence of deformation on myrmekite growth is supported by: absence of comma-shaped myrmekite; absence of relationship between myrmekite presence and inferred finite strain axes; rarity of fine-grained Qtz–Pl fringes around porphyroclasts.

A further textural constraint on the relationship between mylonitic deformation and contact metamorphism is provided by the metapelites interlayered with the granitic mylonites. Figure 6 shows a porphyroblast of andalusite, grown during contact metamorphism; andalusite includes a microboudinaged garnet with well-developed strain shadows, coherent with the orientation of the external, mylonitic foliation. This microstructure shows that development of mylonitic foliation predates contact metamorphism, and suggests that the latter was accompanied by little, or no, deformation of the mylonites. Reactivation of the mylonitic foliation can be observed, accompanied by growth of a thin rim of chlorite around andalusite; both are probably related to a weak retrograde deformation developed in places after contact metamorphism.

MINERAL CHEMISTRY

The composition of minerals was analysed in three mylonite samples with the Cameca Camebax electron microprobe of Centro di Studio per la Geodinamica Alpina, Padova. Working conditions were 15 kV accelerating voltage and 15 nA sample current; natural and synthetic silicates and oxides were used as standards, and matrix effects corrected by the ZAF method. Results are summarised in Table 2, referring to the garnet-bearing sample MC12, phase compositions of which have been utilised in the mass balance calculations below.

There is a marked compositional difference between plagioclase in the fine-grained matrix (Pl_1) and in myrmekite (Pl_2). The former has low anorthite content ($An_{12–17}$), whereas myrmekitic plagioclase varies from An_{10} to An_{40}, with an average of An_{27}. A decrease of anorthite content towards K-feldspar was observed in the majority of myrmekite tubules. The albite component in K-feldspar is commonly in the range 5–8%, but sometimes reaches up to 17%; in this case, the maximum albite content occurs at the edges of porphyroclasts, in proximity of myrmekite.

The various textural generations of muscovite display a subtle, but systematic, variation of phengite content (Fig. 7). On average, the fine-grained mica in the mylonitic foliation has the highest phengite content (up to 6.6 atoms Si), whereas the lamellae associated to myrmekite or K-feldspar approach stoichiometric muscovite (6.1 atoms Si); coarse fish formed from magmatic mica mostly display low phengite substitution (6.1–6.2 atoms Si), but may reach in some cases values of 6.5 atoms Si. These variations are very similar to those reported by Stöckhert (1984) from the granitic orthogneisses outside the contact aureole, in which the mylonitic phengite has been dated at *c.* 100 Ma. The larger scatter of data, and the presence of a third mica generation associated with myrmekite, are the result of younger contact metamorphism. White mica shows random differences in Ti (0.0–0.11 atoms/22 oxygen) and X_{Fe} (0.32–0.86), and low paragonite fraction (<0.08) in all types.

Biotite has $X_{Fe}=0.55$ and *c.* 0.3 atoms Ti in both coarse fish of magmatic origin and fine-grained lamellae of the matrix. Garnet has a grossular component up to 35%, spessartine up to 10%, and X_{Fe} of 0.85–0.95.

In the mylonite sample MC10, utilised in the thermodynamic modelling, phase compositions are identical to those of MC12, with the only difference of a lower value (An_{29}) of the maximum anorthite component of myrmekitic Pl_2.

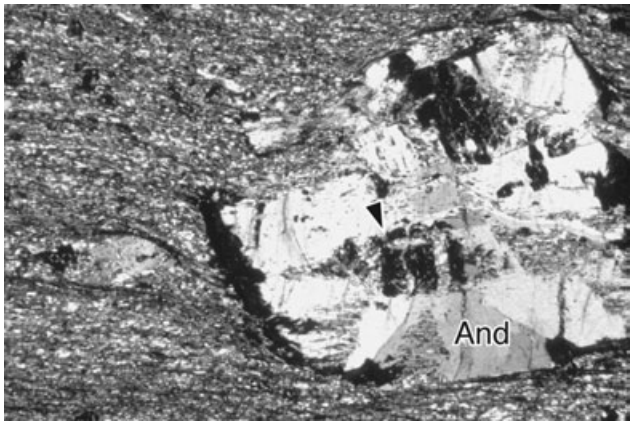

Fig. 6. Andalusite porphyroblast (And) in mylonites of pelitic composition interfingered with the granite-derived mylonites. The lower half of the andalusite includes a microboudinaged crystal of garnet (black, arrow) with strain shadows defined by fine-grained quartz, mica and graphite. Width of view *c.* 3.5 mm CPL.

MASS BALANCE CALCULATIONS

Because the compositions of all the constituent minerals are known, algebraic analysis of the ultramylonite assemblage (Qtz, Kfs, Pl_1, Pl_2, Bt, Ms, Grt) may help reconstruct the reaction of myrmekite growth. The matrix analysis uses the singular value decomposition (SVD) approach introduced by Fisher (1989), which has been applied to identification of metamorphic and melting reactions (e.g. Hartel & Pattison, 1996; Cesare, 2000). It is based on inspection of mass-balance relationships (incompatibilities) in an assemblage matrix in which each column corresponds to one mineral and the rows correspond to the chemical components of the minerals. The method, discussed in detail by Hartel & Pattison (1996) has been first applied in the model CKNASH 'granitic' system by construction of a 7-phase, 5-component matrix, that provides a series of mass balances:

$$[Pl_2]\ 5.0Kfs + 1.58Ms + 0.04Grt = 0.50Pl_1 + 3.93Bt + 2.19Qtz;$$

$$[Pl_1]\ 5.0Kfs + 1.56Ms + 0.08Grt = 0.57Pl_2 + 3.91Bt + 2.26Qtz;$$

$$[Ms]\ 0.52Kfs + 4.32Pl_1 + 0.37Grt = 5.0Pl_2 + 0.26Bt + 0.84Qtz;$$

$$[Bt]\ 0.20Kfs + 4.35Pl_1 + 0.37Grt = 5.0Pl_2 + 0.11Ms + 0.69Qtz.$$

Despite the absence of a unique solution, the mass balances are suggestive of simplified CKNASH relations that consume K-feldspar and garnet and produce

Table 2. Selected electron microprobe analyses of minerals from mylonite sample MC12. 1: matrix plagioclase; 2, 3: myrmekite; 4: myrmekite grain, towards Kfs; 5: same grain, intermediate; 6: same grain, towards matrix; 7, 8: K-feldspar porphyroclast, core and rim, respectively; 9, 10: biotite, fine-grained matrix and coarse fish, respectively; 11: muscovite associated with myrmekite; 12: muscovite fish, 13: fine-grained phengitic mica in the mylonitic matrix; 14, 15: garnet, rim and core, respectively. $X_{Fe} = Fe/(Fe + Mg)$; $X_{An} = Ca/(Ca + Na + K)$.

Phase	Pl_1	Pl_2	Pl_2	Pl_2	Pl_2	Pl_2	Kfs	Kfs	Bt	Bt	Ms	Ms	Ms	Grt	Grt
Id	1	2	3	4	5	6	7	8	9	10	11	12	13	14	15
SiO_2	64.58	59.60	63.34	60.25	59.01	64.01	65.22	65.00	36.14	35.63	45.96	45.96	47.53	37.88	38.29
TiO_2	0.01	0.00	0.02	0.00	0.02	0.00	0.00	0.00	2.82	3.01	0.00	1.14	0.78	0.07	0.08
Al_2O_3	22.06	0.00	23.26	25.19	25.99	21.77	18.51	18.69	17.40	17.57	36.49	34.22	33.16	20.95	21.11
FeO	0.01	0.03	0.02	0.01	0.00	0.00	0.04	0.04	19.46	18.54	1.38	2.10	1.87	26.34	26.70
MnO	0.01	0.02	0.01	0.00	0.02	0.02	0.00	0.00	0.26	0.33	0.00	0.03	0.03	0.10	2.21
MgO	0.00	0.01	0.02	0.01	0.00	0.00	0.00	0.03	8.72	9.27	0.33	1.20	1.45	1.59	2.32
CaO	3.48	7.01	4.93	8.02	8.12	3.46	0.13	0.15	0.02	0.00	0.02	0.01	0.02	12.69	9.47
Na_2O	9.75	7.51	8.88	7.22	6.94	9.71	0.63	1.90	0.10	0.06	0.41	0.36	0.24	0.00	0.00
K_2O	0.09	0.10	0.06	0.09	0.09	0.12	15.33	14.07	9.52	9.52	10.24	10.81	10.83	0.00	0.00
Total	100.02	99.24	100.55	100.80	100.26	99.10	99.89	99.88	94.49	93.99	94.83	95.84	95.94	99.62	100.18
Oxygen	8	8	8	8	8	8	8	8	22	22	22	22	22	24	24
Si	2.85	2.67	2.79	2.67	2.63	2.85	3.00	2.99	5.56	5.50	6.13	6.13	6.31	6.02	6.05
Ti	0.00	0.00	0.00	0.00	0.00	0.00	0.00	0.00	0.33	0.35	0.00	0.11	0.08	0.01	0.01
Al	1.15	1.32	1.21	1.31	1.36	1.14	1.00	1.01	3.15	3.19	5.73	5.38	5.19	3.92	3.93
Fe^{2+}	0.00	0.00	0.00	0.00	0.00	0.00	0.00	0.00	2.50	2.39	0.15	0.23	0.21	3.50	3.53
Mn^{2+}	0.00	0.00	0.00	0.00	0.00	0.00	0.00	0.00	0.03	0.04	0.00	0.00	0.00	0.01	0.30
Mg	0.00	0.00	0.00	0.00	0.00	0.00	0.00	0.00	2.00	2.13	0.06	0.24	0.29	0.38	0.55
Ca	0.16	0.34	0.23	0.38	0.39	0.16	0.01	0.01	0.00	0.00	0.00	0.00	0.00	2.16	1.60
Na	0.83	0.65	0.76	0.62	0.60	0.84	0.06	0.17	0.03	0.02	0.11	0.09	0.06	0.00	0.00
K	0.00	0.01	0.00	0.01	0.01	0.01	0.90	0.82	1.87	1.87	1.74	1.84	1.83	0.00	0.00
X_{An}	0.16	0.34	0.23	0.38	0.39	0.16									
X_{Fe}									0.56	0.53	0.70	0.50	0.42	0.90	0.87

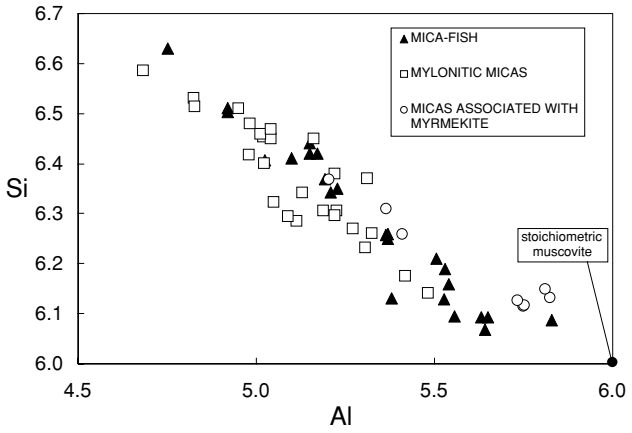

Fig. 7. Si vs. Al diagram for white mica in the pegmatitic ultramylonites; see text for explanation.

plagioclase, biotite and quartz, a result consistent with the observed microstructures of K-feldspar replacement by myrmekite and crystallization of biotite in the matrix. Note that muscovite may occur both on the reactant and product sides, based on the presence of biotite in the balance.

However, because Fe and Mg are required by the presence of biotite and garnet, a complete modelling needs treatment of the full FMCKNASH system: in this case, no mass balance relationships can be obtained, indicating high variance of the observed assemblage in the full chemical system. This suggests that the above relations in the simplified CKNASH are only first-order approximations of the actual myrmekite-forming reaction, which is likely to be obscured by the consumption of one or more reactants (e.g. chlorite and/or epidote, see below).

THERMODYNAMIC MODELLING OF MODAL CHANGES

The changes in modal composition as a function of *P–T* have been modelled with the Perple_X computer program (Connolly, 1990), using the thermodynamic data of Holland & Powell (1998), and taking into account the following solutions: chlorite ($Mg_{(5-y)x}Fe_{(5-y)(1-x)}Al_{4+2y}Si_{3-y}O_{10}(OH)_8$, Holland *et al.*, 1998); biotite ($KMg_{(3-y)x}Fe_{(3-y)(1-x)}Al_{1+2y}Si_{3-y}O_{10}(OH)_2$, Holland & Powell, 1998); staurolite ($Mg_{4x}Fe_{4-4x}Al_{18}Si_{7.5}O_{48}H_4$, nonideal, Holland & Powell, 1998); muscovite ($K_xNa_{1-x}Mg_yFe_zAl_{3-2(y+z)}Si_{3+y+z}O_{10}(OH)_2$, modified from Chatterjee & Froese, 1975 and Holland & Powell, 1998); sanidine ($K_xNa_{1-x}AlSi_3O_8$, Thompson & Waldbaum, 1969); albite/microcline ($Na_xK_yCa_{1-x-y}Al_{2-x-y}Si_{2+x+y}O_8$, Newton *et al.*, 1980 and Thompson & Waldbaum 1969); plagioclase ($Na_xCa_{1-x}Al_{2-x}Si_{2+x}O_8$, Newton *et al.*, 1980); garnet ($Fe_{3x}Ca_{3y}Mg_{31-x-y}Al_2Si_3O_{12}$, nonideal, Holland & Powell, 1998); clinopyroxene ($Na_{1-y}Ca_yMg_{xy}Fe_{1-xy}Al_ySi_2O_6$, modified from Gasparik, 1985). The model calculations assume the presence of a pure water fluid and that all iron is present as Fe^{3+}. As discussed in the introduction, the age of the granitic protolith of mylonites is late-Variscan (*c.* 260 Ma); this restricts our considerations to the Alpine *P–T* path of the area.

Using the P–T(–t) data of Stöckhert (1984, 1987) and Cesare (1992, 1994), the Alpine P–T path used in the calculation consists of a decompression/cooling phase starting with eo-Alpine conditions (point A), followed by isobaric (2.75 kbar) heating to 530 °C, the estimated peak temperature of Oligocene contact metamorphism (point C). P–T values at point C are derived from the AFM mineral assemblage And–St–Bt–Chl, present within the metapelites interlayered with the mylonites. Figure 8 summarises the results of the modelling applied to sample MC10; calculations for other measured bulk compositions show similar features to those obtained for MC10. Regardless of the uncertainties in the approach and the assumed P–T path, the phase equilibrium model suggests that the growth of plagioclase and biotite at the expense of muscovite and K-feldspar is an almost inescapable consequence of contact metamorphism. Although chlorite and epidote are not observed in the studied samples, these minerals were probably stable during the initial stages of contact metamorphism, as predicted by the equilibrium model and as observed by Stöckhert (1987) and Borsi et al. (1980) in similar orthogneisses beyond the aureole. The transition from the regional metamorphic stage (A) to contact metamorphism (C) shows an increase of K-feldspar, followed by a sudden drop, and a net increase of plagioclase; during the heating path, at *c.* 450 °C, a major change in modal composition is expected via the divariant devolatilization reaction

$$\mathrm{Kfs + Chl + Ep \rightarrow Pl + Bt + Ms + Qtz + H_2O},$$

which is consistent with replacement of K-feldspar by myrmekite. The calculations also indicate that albite is the stable plagioclase composition along the entire decompression path, and that only during the isobaric heating, from about 400 °C, does anorthite content increase to oligoclase-andesine compositions (up to 40% An) as epidote is consumed.

The only difference between the calculated and the observed modal compositions is the presence of minor clinopyroxene, which is computed to be stable during most of the decompressional path, but which is not observed (Stöckhert, 1987). Owing to the presence of garnet in the orthogneisses, the natural phase equilibria most probably reflect the role of Mn, which stabilizes garnet relative to clinopyroxene, but which was not included in the model system. Despite this discrepancy, the thermodynamic calculation shows remarkable agreement with petrographic and compositional data from the granitic ultramylonites. In particular, the calculated model assemblage Qtz–Pl($An_{30–40}$)–Kfs–Bt(Ann_{55})–Ms, matches the measured compositions of recrystallized phases (myrmekitic plagioclase, biotite and muscovite) in the mylonites. Because the recrystallized assemblage is only stable during the isobaric heating path at $T > 450$ °C, we conclude that myrmekite formation was related to the contact metamorphic event.

DISCUSSION

Contact metamorphic origin of myrmekite coronas

The mylonitic gneisses contain extensive evidence of crystallization under static conditions that overprinted a former ultramylonite fabric. The evidence includes the straight shape, homogeneous distribution and random crystallographic orientation of myrmekite tubules in the corona, the grain growth processes in quartz ribbons, and the random orientation of newly formed quartz, biotite and muscovite in the mylonite matrix. Based on (i) absence of myrmekites in analogous orthogneisses outside the contact aureole (Stöckhert, 1987) and (ii) comparison with microstructures of interlayered metapelites, we associate this static event with the Oligocene metamorphism in the contact aureole of Cima di Vila.

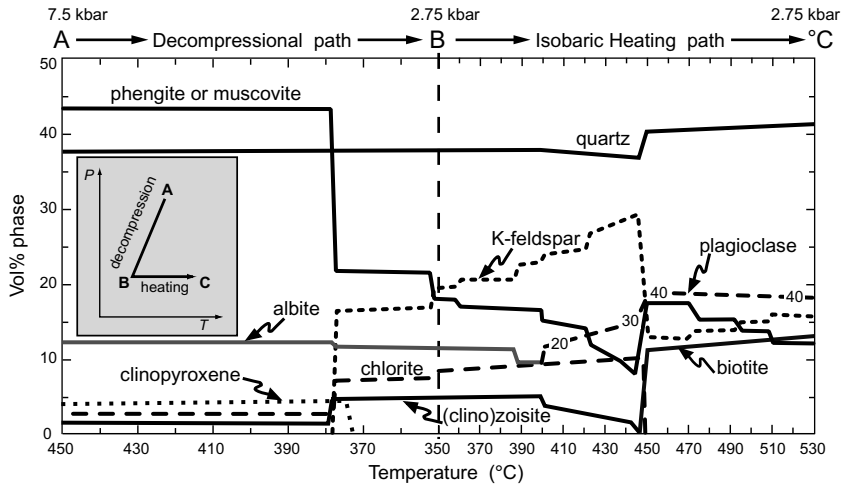

Fig. 8. Changes of phase proportions (in vol.%) calculated for sample MC10 along the inferred decompression (A–B) and heating (B–C) P–T path of Alpine metamorphism (inset). Numbers along plagioclase curve indicate calculated anorthite content.

This interpretation is supported by the results of thermodynamic modelling, which show: (i) a close match between the measured phase compositions in the ultramylonites (particularly of plagioclase and biotite) and the values calculated at the estimated P–T conditions of contact metamorphism; (ii) the metastability of the assemblage Qtz–Kfs–Bt–Ms–Pl($An_{>20}$) during the entire decompressive path of Alpine regional metamorphism.

A static (contact) metamorphic scenario explains the peculiar distribution of myrmekite in the ultramylonites. Corona textures are typical of static environments, and attest to preferred nucleation at grain contacts between the reactant phases, and to diffusion-controlled growth process. Because K-feldspar is the reactant that is consumed in the highest amounts during the proposed myrmekite growth reaction, and because of the similar Al and Si contents of K-feldspar and myrmekite, preferred growth of myrmekite replacing K-feldspar is to be expected. This preference is observed in most myrmekite-bearing rocks. In the studied example, nucleation of myrmekite appears to have occurred, without controls by the neighbouring phase, along the entire boundary of elliptical K-feldspar. Nucleation was followed by preferred growth towards the receding K–feldspar boundary, causing initial impingement of myrmekite grains, and further growth as coalescent tubules orthogonal to the initial K–feldspar grain boundary.

Timing relationships between mylonitisation and contact metamorphism

The static metamorphism and myrmekite development may have occurred immediately after the mylonitic deformation of the granitic pegmatites, as frequently the case during post-kinematic annealing of high-T mylonites, or during a completely independent, younger metamorphic stage. Several constraints, that emerge from field, petrologic and geochronologic data, favour the second hypothesis:

1 The myrmekite-bearing ultramylonites contain the same textural generations of white mica, with the same chemical composition, as those observed in similar pegmatitic orthogneisses located beyond the contact aureole. In those rocks, the fine-grained phengite associated with the mylonitic foliation gives an age of *c.* 100 Ma (Stöckhert, 1984), which suggests an eo-Alpine mylonitisation event.

2 The isoclinal folding of the main foliation, that affected the mylonitic foliation in the studied area, is widespread throughout the basement north of the DAV line and has been modelled as a late-Alpine overprint on the eo-Alpine fabric (Mager, 1985; Kleinschrodt, 1987; Stöckhert, 1987). This folding phase predates the contact metamorphism.

3 The microstructures associated with mylonites located further away from the Oligocene intrusives are indicative of relatively low-temperature conditions (*c.* 450 °C, Stöckhert, 1987), that are inconsistent with the higher temperatures (*c.* 530 °C) attained during contact metamorphism.

Based on these constraints, we consider the mylonitic deformation and contact metamorphism as two separate events, the former of eo-Alpine age (*c.* 100 Ma), and the latter Oligocene (30 ± 3 Ma).

Myrmekite, deformation and fluids

Myrmekite is frequently observed in deformed granitoids, and particularly around porphyroclasts in augengneisses (e.g. Simpson, 1985); this has led to the suggestion of a correlation between crystal-plastic deformation and myrmekite development (discussion in Simpson & Wintsch, 1989 and Vernon, 1991). Despite some analogies between the subject of this study and the microstructures interpreted by Simpson & Wintsch (1989) as deformation-induced, we can confidently rule out an active role of deformation during growth of the studied myrmekite coronas. In fact, the coronas are continuous and of constant thickness, myrmekite tubules are straight, the plagioclase host is untwinned, transition from myrmekite to Qtz–Pl aggregates is rare, and, conversely, static grain growth in the matrix widespread.

This observation is in agreement with the conclusions of Vernon (1991) on the absence of a general genetic relationship between strain and myrmekite growth in deformed rocks. However, this conclusion does not imply that the model of Simpson & Wintsch (1989) is not valid in particular instances. Although Vernon (2000) lists myrmekite among the textural markers of subsolidus deformation of granitoids, he considers deformation as a prerequisite, rather than the driving force or a necessary element during myrmekite growth. In this regard, we do not exclude the possibility that strain energy concentrations preserved at the surfaces of K-feldspar porphyroclasts may have contributed to the preferred nucleation of myrmekite.

In his discussion on the role of stress and strain energy on the nucleation and growth of myrmekite in deformed rocks, Vernon (1991) proposes that deformation may catalyse the kinetics of myrmekite growth by favouring the access of intergranular fluids to the K-feldspar–plagioclase grain boundary. Our results suggest an additional mechanism, that may be active with or without deformation, namely the progress of devolatilisation reactions. The proposed reaction of myrmekite formation

$$\mathrm{Kfs} + \mathrm{Chl} + \mathrm{Ep} \rightarrow \mathrm{Pl} + \mathrm{Bt} + \mathrm{Ms} + \mathrm{Qtz} + \mathrm{H_2O},$$

releases fluid by decomposition of chlorite and epidote. This fluid, available throughout the fine-grained mylonite matrix, can act in a similar manner as discussed by Vernon (1991). Even in the absence of crystal-plastic deformation, fluid presence at advancing myrmekite tips (i.e. far from the loci of fluid release) can be

expected owing to the volume decrease and porosity increase related to the replacement of K-feldspar by myrmekite (e.g. Simpson & Wintsch, 1989). Fluid filled pores, a common feature in alkali feldspar from granitoid rocks and their metamorphic derivatives (e.g., Walker et al., 1995 and references therein), are an additional potential source of fluid.

Prograde origin of myrmekite associated with muscovite

Association of muscovite with myrmekite has generally been regarded as evidence of retrograde metamorphism (e.g. Ashworth, 1972; Phillips *et al.*, 1972), possibly accompanied by metasomatic alteration (Phillips, 1980). Muscovite is associated with the studied myrmekite in the coronas around K-feldspar. The euhedral shape of muscovite, the frequent rational phase boundaries towards plagioclase, and the chemical composition with low phengite content indicate that myrmekite and muscovite are coeval and crystallized together replacing K-feldspar.

However, our thermodynamic modelling, summarised in Fig. 8 shows that conditions for myrmekite growth in the ultramylonites are achieved during the isobaric heating path associated with contact metamorphism. At about 450 °C, the former greenschist facies gneiss, characterised by the assemblage Qtz–Phe–Kfs–Ab–Chl–Ep, is predicted to react to the assemblage Qtz–Pl–Ms–Kfs–Bt, with a net production of *c.* 10% muscovite. After this sudden change, the mineral composition shows small variations, with consumption of muscovite and increase of anorthite in plagioclase, up to the final temperature of 530 °C. Thus, we believe that the association of myrmekite with muscovite is not proof of retrograde metamorphism. The frequent occurrence of myrmekite and muscovite in retrograde settings may in many cases merely indicate the superposition of a tectonometamorphic event on the primary magmatic association. In the case of a single metamorphic event, or during the cooling of the granitoid, the conditions must be of lower temperature, if compared to the magmatic stage. Alternatively, when plutonic rocks are involved in complex, polymetamorphic *P–T–t* histories, there are no restrictions to the formation of myrmekite associated with muscovite during prograde (up-temperature) events.

As concerns the 'metasomatic' character of myrmekite replacing K-feldspar, our mass-balance calculations and thermodynamic modelling suggest that in the studied example this process may take place isochemically (see also Simpson & Wintsch, 1989). In this case, loss and gain of elements (particularly Ca, Na & K) at myrmekite growth sites can be balanced by simultaneous reactions and crystallization in the matrix, in a way that maintains the system closed on a scale of centimetres.

CONCLUSIONS

This work adds further information and complexity to the genetic interpretation of myrmekite in deformed granitoid rocks. The observed myrmekite coronas around K-feldspar porphyroclasts are related to a static crystallization event, and are not deformation-induced as it is in some mylonitic granitoids. The static crystallization was the result of Oligocene contact metamorphism in the aureole of Cima di Vila, which occurred at *c.* 2.5–3 kbar and *c.* 530 °C. In the example studied, despite close association with muscovite, myrmekite forms during prograde (up-temperature) metamorphism, via a reaction of the type

$$\mathrm{Kfs} + \mathrm{Chl} + \mathrm{Ep} \rightarrow \mathrm{Pl} + \mathrm{Bt} + \mathrm{Ms} + \mathrm{Qtz} + \mathrm{H_2O}.$$

The agreement of observed mineral compositions and abundances with predictions based on thermodynamic calculations, along with existence of CKNASH mass balance relations among corona and adjacent matrix, supports our contention that myrmekite can develop in a closed system, of thin-section scale, without involving larger scale metasomatic exchange.

ACKNOWLEDGEMENTS

Financial support from University of Padova, Fondi Progetti Ricerca 1998 (ACNE), from C.N.R. and from C.A.R.G — P.A.B. The manuscript benefited from discussions with G. Di Toro, N. Mancktelow, A. Mignucci and G. Pennacchioni, from kind help of R. Fontarnau, P. Martinez and L. Montserrat during the stay of CM at Barcelona, and from technical assistance of R. Carampin during EMP analyses at C.N.R. CSGA — Padova. We wish to thank B. Stöckhert and R. Wintsch for their constructive reviews, and the convenors of the microstructural and metamorphic sessions at the Ron Vernon Symposium, for giving us the opportunity to present this paper.

REFERENCES

Ashworth, J. R., 1972. Myrmekites of exsolution and replacement origins. *Geological Magazine*, **109,** 45–62.

Ashworth, J. R., 1986. Myrmekite replacing albite in prograde metamorphism. *American Mineralogist*, **71,** 895–899.

Becke, F., 1908. Über Myrmekite. *Schweizerische Mineralogische und Petrographische Mitteilungen*, **27,** 377–390.

Bellieni, G., 1980. The Cima di Villa (Zinsnock) massif: geochemical features and comparisons with the Vedrette di Ries (Rieserferner) pluton (Eastern Alps — Italy). *Neues Jahrbuch für Mineralogie, Abhandlungen*, **138,** 244–258.

Bellieni, G., Peccerillo, A. & Poli, G., 1981. The Vedrette di Ries (Rieserferner) Plutonic Complex: Petrological and geochemical data bearing on its genesis. *Contributions to Mineralogy and Petrology*, **78,** 145–156.

Borsi, S., Del Moro, A., Sassi, F. P., Visonà, D. & Zirpoli, G., 1980. On the existence of Hercynian aplites and pegmatites in the lower Aurina valley (Ahrntal, Austrides, Eastern Alps). *Neues Jahrbuch für Mineralogie, Monatshefte*, **11,** 501–514.

Borsi, S., Del Moro, A., Sassi, F. P. & Zirpoli, G., 1979. On the age of the Vedrette di Ries (Rieserferner) massif

and its geodynamic significance. *Geologische Rundschau*, **68,** 41–60.

Cesare, B., 1992. Metamorfismo di contatto di rocce pelitiche nell'aureola di Vedrette di Ries (Alpi Orientali — Italia) *PhD Thesis, University Padova*, Padova, Italy.

Cesare, B., 1994. Hercynite as the product of staurolite decomposition in the contact aureole of Vedrette di Ries, eastern Alps, Italy. *Contributions to Mineralogy and Petrology*, **116,** 239–246.

Cesare, B., 1999. Multi-stage pseudomorphic replacement of garnet during polymetamorphism: 1. Microstructures and their interpretation. *Journal of Metamorphic Geology*, **17,** 723–734.

Cesare, B., 2000. Incongruent melting of biotite to spinel in a quartz-free restite at El Joyazo (SE Spain): Textures and reaction characterization. *Contributions to Mineralogy and Petrology*, **139,** 273–284.

Chatterjee, N. D. & Froese, E., 1975. A thermodynamic study of the pseudo-binary join muscovite-paragonite in the system $KAlSi_3O_8$–$NaAlSi_3O_8$–Al_2O_3–SiO_2–H_2O. *American Mineralogist*, **60,** 985–993.

Connolly, J. A. D., 1990. Multivariable phase diagrams: an algorithm based on generalized thermodynamics. *American Journal of Science*, **290,** 666–718.

Fisher, G. W., 1989. Matrix analysis of metamorphic mineral assemblages and reactions. *Contributions to Mineralogy and Petrology*, **102,** 69–77.

Gasparik, T., 1985. Experimental study of subsolidus phase relations and mixing properties of pyroxene and plagioclase in the system Na_2O–CaO–Al_2O_3–SiO_2. *Contributions to Mineralogy and Petrology*, **89,** 346–357.

Hartel, T. H. D. & Pattison, D. R. M., 1996. Genesis of the Kapuskasing (Ontario) migmatitic mafic granulites by dehydration melting of amphibolite: the importance of quartz to reaction progress. *Journal of Metamorphic Geology*, **14,** 591–611.

Hippertt, J. F. & Valarelli, J. V., 1998. Myrmekite: constraints on the available models and a new hypothesis for its formation. *European Journal of Mineralogy*, **10,** 317–331.

Holland, T. J. B., Baker, J. & Powell, R., 1998. Mixing properties and activity-composition relationships of chlorites in the system MgO–FeO–Al_2O_3–SiO_2–H_2O. *European Journal of Mineralogy*, **10,** 395–406.

Holland, T. J. B. & Powell, R., 1998. An internally consistent thermodynamic data set for phases of petrological interest. *Journal of Metamorphic Geology*, **16,** 309–343.

Kleinschrodt, R., 1987. Quarzkorngefugeanalyse im Altkristallin südlich des westlichen Tauernfensters (Südtirol/Italien). *Erlanger Geologische Abhandlungen*, **114,** 1–82.

Mager, D., 1985. Geologische und petrographische Untersuchungen am Südrand des Rieserferner — Pluton (Südtirol) unter Berücksichtigung des Intrusionsmechanismus. *PhD Thesis, University Erlangen*, Erlangen, Germany.

Müller, W., Mancktelow, N. S. & Meier, M., 2000. Rb-Sr microchrons of synkinematic mica in mylonites: an example from the DAV fault of the Eastern Alps. *Earth and Planetary Science Letters*, **180,** 385–397.

Newton, R. C., Charlu, T. V. & Kleppa, O. J., 1980. Thermochemistry of the high structural state plagioclases. *Geochimica Cosmochimica Acta*, **44,** 933–941.

Phillips, E. R., 1974. Myrmekite-one hundred years later. *Lithos*, **7,** 181–194.

Phillips, E. R., 1980. On polygenetic myrmekite. *Geological Magazine*, **17,** 29–36.

Phillips, E. R., Ransom, D. M. & Vernon, R. H., 1972. Myrmekite and muscovite developed by retrograde metamorphism at Broken Hill, New South Wales. *Mineralogical Magazine*, **38,** 570–578.

Prochaska, W., 1981. Einige Gangesteine der Rieserferner Intrusion mit neuen radiometrischen Altersdaten. *Mitteilungen der Gesellschaft der Geologie und Berbaustudent, Wien*, **27,** 161–171.

Sassi, F. P., Zanettin, B. & Zirpoli, G., 1980. Quadro della storia termica Alpina nelle Alpi Orientali. *Rendiconti SIMP*, **36,** 19–33.

Schmid, S. M., Aebli, H. R., Heller, F. & Zingg, A., 1989. The role of the Periadriatic Line in the tectonic evolution of the Alps. In: *Alpine Tectonics. Special Publications, 45*, (eds Coward, M. P., Dietrich, D. & Park, R. G.), pp. 153–171. Geological Society of America, Boulder.

Schwantke, A., 1909. Die Beimischung von Ca im Kalifeldspat und die Myrmekitibildung. *Zentralblatt für Geologie und Paläontologie*, **1,** 311–316.

Simpson, C., 1985. Deformation of granitic rocks across the brittle-ductile transition. *Journal of Structural Geology*, **7,** 503–511.

Simpson, C. & Wintsch, R. P., 1989. Evidence for deformation-induced K-feldspar replacement by myrmekite. *Journal of Metamorphic Geology*, **7,** 261–275.

Steenken, A., Siegesmund, S. & Heinrichs, T., 2000. The emplacement of the Rieserfener Pluton (Eastern Alps, Tyrol): constraints from field observations, magnetic fabrics and microtextures. *Journal of Structural Geology*, **22,** 1855–1873.

Stöckhert, B., 1984. K-Ar determinations on muscovites and phengites from deformed pegmatites, and the minimum age of the Old Alpine deformation in the Austridic basement to the south of the western Tauern window (Ahrn valley, Southern Tyrol, Eastern Alps). *Neues Jahrbuch für Mineralogie, Abhandlungen*, **150,** 103–120.

Stöckhert, B., 1987. Das Uttenheimer Pegmatit-Feld (Ostalpines Altkristallin, Süditirol) Genese und alpine Überprägung. *Erlanger Geologische Abhandlungen*, **114,** 83–106.

Thompson, J. B. & Waldbaum, D. R., 1969. Mixing properties of sanidine crystalline solutions. IV. Phase diagrams from equations of state. *American Mineralogist*, **76,** 493–500.

Vernon, R. H., 1978. Pseudomorphous replacement of cordierite by symplectic intergrowths of andalusite, biotite and quartz. *Lithos*, **11,** 283–289.

Vernon, R. H., 1991. Questions about myrmekite in deformed rocks. *Journal of Structural Geology*, **13,** 979–985.

Vernon, R. H., 2000. Review of Microstructural Evidence of Magmatic and Solid-State Flow. *Electronic Geosciences*, **5,** 2.

Walker, F. D. L., Martin, R. L. & Parson, I., 1995. Micropores and micropermeable texture in alkali feldspars: geochemical and geophysical implications. *Mineralogical Magazine*, **59,** 505–534.

Received 7 November 2000; revision accepted 9 May 2001